UNCLASSIFIED

Technical Report #52

(1)

SI

AD-A205 747

ORT DOCUMENTATION PAGE

1a	1b. RESTRICTIVE MARKINGS: NA
2a. SECURITY CLASSIFICATION AUTHORITY: NA	3. DISTRIBUTION / AVAILABILITY OF REPORT: Distribution Unlimited; Approved for Public Release
2b. DECLASSIFICATION / DOWNGRADING SCHEDULE: NA	
4. PERFORMING ORGANIZATION REPORT NUMBER(S)	5. MONITORING ORGANIZATION REPORT NUMBER(S): NA
6a. NAME OF PERFORMING ORGANIZATION: Indiana University	6b. OFFICE SYMBOL (If applicable): NA
7a. NAME OF MONITORING ORGANIZATION: ONR	
6c. ADDRESS (City, State, and ZIP Code): Department of Chemistry, Bloomington, IN 47405	7b. ADDRESS (City, State, and ZIP Code): 800 N. Quincy Street, Arlington, VA 22217
8a. NAME OF FUNDING / SPONSORING ORGANIZATION	8b. OFFICE SYMBOL (If applicable)
9. PROCUREMENT INSTRUMENT IDENTIFICATION NUMBER: Contract N00014-86-K-0366	
8c. ADDRESS (City, State, and ZIP Code)	10. SOURCE OF FUNDING NUMBERS

PROGRAM ELEMENT NO.	PROJECT NO.	TASK NO.	WORK UNIT ACCESSION NO
		R&T Code 4134006	

11. TITLE (Include Security Classification): Simultaneous Measurement of Spatially Resolved Electron Temperatures, Electron Number Densities and Gas Temperatures by Laser Light Scattering from the ICP

12. PERSONAL AUTHOR(S): M. Huang, G.M. Hieftje

13a. TYPE OF REPORT	13b. TIME COVERED	14. DATE OF REPORT (Year, Month, Day)	15. PAGE COUNT
Technical	FROM ____ TO ____	February 10, 1989	38

16. SUPPLEMENTARY NOTATION

17. COSATI CODES		
FIELD	GROUP	SUB-GROUP

18. SUBJECT TERMS (Continue on reverse if necessary and identify by block number): Inductively Coupled Plasma · Rayleigh Scattering, Combination Diagnostics · Thomson Scattering

19. ABSTRACT (Continue on reverse if necessary and identify by block number)

Spatially resolved electron temperatures, electron number densities and gas-kinetic temperatures have been determined at five obervation heights, nine radial positions, and two settings of RF input power in an aerosol-free argon ICP sustained with a commercial MAK torch. The measurements were obtained by means of simultaneous ruby-laser Thomson scattering the Rayleigh scattering. In the central channel of the ICP the electron temperature ranges from 7000 K to 8500 K, the gas kinetic temperature is about 1000 K to 2000 K lower than the electron temperature, and the electron number density varies from 1.9 to 7.0 x 10^{15} cm^{-3}. Among the measured parameters, the electron number density is most sensitive to the input RF power and is noticeable higher than the LTE value determined from the measured electron temperature and the Saha equation. The overpopulation of electrons can be probably be attributed to fast ambipolar diffusion and slow ion-electron recombination processes, resulting in a recombining plasma in the analytical zone. This non-LTE feature might be significant for excitation and ionization mechanisms in the ICP.

20. DISTRIBUTION / AVAILABILITY OF ABSTRACT	21. ABSTRACT SECURITY CLASSIFICATION
☒ UNCLASSIFIED/UNLIMITED ☐ SAME AS RPT ☐ DTIC USERS	Distribution Unlimited

22a. NAME OF RESPONSIBLE INDIVIDUAL	22b. TELEPHONE (Include Area Code)	22c. OFFICE SYMBOL
Gary M. Hieftje	(812) 335-2189	

DD FORM 1473, 84 MAR — 83 APR edition may be used until exhausted. All other editions are obsolete.

SECURITY CLASSIFICATION OF THIS PAGE: UNCLASSIFIED

X for the full paper/cc

Simultaneous Measurement of Spatially Resolved Electron Temperatures, Electron Number Densities and Gas Temperatures by Laser Light Scattering from the ICP

Mao Huang* and Gary M. Hieftje+

Department of Chemistry

Indiana University

Bloomington, IN 47405

*On leave from:
Department of Physics
The Branch School of Peking University
Beijing, China

+Author to whom correspondence should be addressed.

Abstract -- Spatially resolved electron temperatures, electron number densities and gas-kinetic temperatures have been determined at five observation heights, nine radial positions, and two settings of RF input power in an aerosol-free argon ICP sustained with a commercial MAK torch. The measurements were obtained by means of simultaneous ruby-laser Thomson scattering and Rayleigh scattering. In the central channel of the ICP the electron temperature ranges from 7000 K to 8500 K, the gas kinetic temperature is about 1000 K to 2000 K lower than the electron temperature, and the electron number density varies from 1.9 to 7.0 x 10^{15} cm^{-3}. Among the measured parameters, the electron number density is most sensitive to the input RF power and is noticeably higher than the LTE value determined from the measured electron temperature and the Saha equation. The overpopulation of electrons can probably be attributed to fast ambipolar diffusion and slow ion-electron recombination processes, resulting in a recombining plasma in the analytical zone. This non-LTE feature might be significant for excitation and ionization mechanisms in the ICP.

1. INTRODUCTION

If the inductively coupled argon plasma (ICAP) sustained at atmospheric pressure were in thermodynamic equilibrium (TE), a single physical parameter (e.g. temperature T or electron number density n_e) would be sufficient to completely describe its behavior. That is, under TE conditions, electron number density, the number density of ions at different ionization stages, energy-level populations, the frequency distribution of radiation and the velocity distribution of all species could be all exactly determined from the ideal gas law, the Boltzmann distribution, the Saha equation, Planck's radiation law and the Maxwell distribution.

If the ICAP is not in TE, but were instead in local thermodynamic equilibrium (LTE), it could again be described by only one physical parameter. However, the parameter would be a function of spatial position e.g. $T(r,z)$ or $n_e(r,z)$, where r and z are radial position and observation height, respectively. For a given spatial point (r,z), all the detailed information mentioned above (except the Planck radiation law) could be determined by $T(r,z)$ or $n_e(r,z)$, using the same equations or laws as for the case of TE. Unfortunately, as pointed out quite early by many investigators [1-5], the ICAP is not in LTE either. Thus, even at a given spatial point, a single physical parameter is not sufficient to describe the plasma behavior. Of course, analyte excitation might be attributable to the presence or concentration of particular species (e.g. Ar or Ar^+). However, measuring the concentrations of such species alone does not characterize the plasma as a whole and might not even elucidate analyte-excitation events. The key question then is, "What are the most useful fundamental parameters for characterizing the behavior of the ICAP?". The answer is: local

electron temperature $T_e(r,z)$, electron number density $n_e(r,z)$ and gas-kinetic temperature $T_g(r,z)$.

The reasons for this conclusion are compelling. When the sample aerosol is introduced into a plasma through the central channel, the first events involved are desolvation, vaporization and dissociation, which are greatly affected by the gas temperature T_g. Electron temperature T_e and electron number density n_e, on the other hand, are the determining parameters for electrical conductivity and ambipolar diffusion in the plasma. Two other important transport coefficients - thermal conductivity and viscosity - are controlled by T_e, n_e and T_g [6].

Furthermore, T_e and n_e are extremely important in evaluating a variety of plausible analyte excitation and ionization mechanisms in the ICAP. First, the rate constants for collisional excitation, de-excitation, ionization and three-body recombination are generally sensitive to T_e, and are all proportional to n_e (except for three-body recombination which is proportional to the square of n_e [7-9]). There is little doubt that when both T_e and n_e are high, electron impact will dictate the energy-level populations of analyte atoms and ions, and should play a vital part in the excitation and ionization processes. Of course, the Boltzmann distribution and the Saha equation may not apply to such events, as n_e might not be the LTE value corresponding to T_e. Secondly, Penning ionization would contribute to analyte ionization and excitation only when argon metastable levels are highly populated [2]; this event would occur only when electrons are overpopulated with respect to T_e [10]. Thirdly, charge transfer, which has recently been suggested to play a significant role in the ICP [11,12], is indirectly influenced by T_e and n_e. If T_e is quite high, many elements would be ionized mostly by electron impact, and only a small portion of the

analyte species would remain as atoms. Thus, charge transfer would not contribute appreciably to the degree of ionization. On the other hand, if electrons are overpopulated and T_e remains relatively low, charge transfer might be of importance.

From the above discussion, local T_e, n_e and T_g values are critical in describing the macroscopic behavior and microscopic processes that occur in the ICP. It is therefore not surprising that many authors have measured these parameters using different methods of plasma diagnostics [1,3-5,13-35]. Among these methods, laser light scattering offers a number of unique advantages [36-39]. Most importantly, when a focused laser beam is scattered by the plasma, both Thomson scattering and Rayleigh scattering can be measured at the same time, making possible the simultaneous measurement of T_e, n_e and T_g, on a spatially and temporally resolved basis. These procedures greatly reduce the errors generated by the Abel inversion required by most other methods and avoid the plasma drift (instability) problem, at least for any chosen spatial point of the measurements.

In the present paper, we report local values of T_e, n_e and T_g measured simultaneously by means of Thomson scattering and Rayleigh scattering from an aerosol-freeICAP sustained with a commercial MAK torch. The measurements were performed at five observation heights (5.0, 7.5, 10.0, 12.5, and 15.0 mm above the load coil (ALC)) and at nine radial positions (-6.0, -4.5, -3.0, -1.5, 0, 1.5, 3.0, 4.5 and 6.0 mm from the plasma axis). Two settings of RF input power (0.75 and 1.0 kW) were used for comparison. Compared to the results of a previous study [28], the T_e and n_e values presented here should be more reliable, because a new data treatment procedure has been used (see next section). In addition, no aerosol nor analyte was present in the central-gas flow so that the error in T_e values determined by using the

ideal gas law and Rayleigh scattering has been minimized. Theoretical formulas employed in the calculations of T_e, n_e and T_g from the scattered light signals will be briefly reviewed, and some new calibration and normalization procedures for the multichannel Thomson scattering system will be described. Finally, the experimental results will be discussed and conclusions will be drawn.

2. THEORY

In this section, the theoretical formulas used for calculating T_e, n_e and T_g from the measured Thomson-scattering and Rayleigh-scattering signals will be briefly summarized. For a more detailed discussion of the theory from which the formulas are derived, the reader is referred to earlier papers [35,39].

A Thomson-scattering signal $I(\lambda)$, expressed as a function of wavelength λ is related to the shift $\Delta\lambda$ from the incident laser wavelength λ_o by the formula

$$\ln I(\lambda) = C - \frac{m_e c^2}{8kT_e \sin^2(\theta/2) \cdot \lambda_o^2} \cdot (\Delta\lambda)^2 \qquad (1)$$

where C is a constant that depends on the entire scattering system, m_e is the mass of an electron, c the speed of light, k the Boltzmann constant, and θ the angle between the observation direction and the laser incident beam. According to Eqn (1), the local electron temperature T_e can be determined from the slope of a plot of $\ln I(\lambda)$ vs. $(\Delta\lambda)^2$. To use Eqn (1), one must be sure that $m_e c^2$ and kT_e are in the same units, no matter whether T_e is in eV or in K. The same is true of course for $(\Delta\lambda)^2$ and λ^2_o.

Because the amplitude of the entire Thomson-scattering spectrum is proportional to the electron number density, the sum of the absolutely calibrated signals from all spectral channels can be used to calculate the local value of n_e as shown in Eqn (2).

$$n_e = n_A \cdot \frac{\int I(\lambda)d\lambda}{I_{RA}} \cdot \frac{\sigma_{RA}}{\sigma_T} , \qquad (2)$$

where n_A is the number density of argon atoms at the temperature at which the Rayleigh-scattering measurement is performed (usually room temperature [35,39]), the integration term expresses the sum of Thomson-scattering signals from all spectral channels, I_{RA} is the Rayleigh-scattering signal from the central spectral channel located at the incident laser wavelength, σ_{RA} is the Rayleigh-scattering cross section of argon gas, and σ_T is the Thomson-scattering cross section. In Eqn (2), Rayleigh scattering serves to calibrate on an absolute basis the Thomson scattering signals [35,39].

When the plasma is on, the Rayleigh-scattering signal will be greatly reduced compared to that when the plasma is off. This is because the magnitude of the Rayleigh signal is proportional to the argon-atom number density which, in turn, is inversely proportional to the gas temperature according to the ideal gas law. Therefore, the ratio of the Rayleigh-scattering signal when the plasma is off $I_{RA(off)}$ to that when the plasma is on $I_{RA(on)}$ can be used to determine the local gas temperature according to Eqn (3).

$$T_g = \frac{I_{RA(off)}}{I_{RA(on)}} \cdot T_{room} \quad , \tag{3}$$

where T_{room} is the room temperature at which $I_{RA(off)}$ is measured. Note that in Eqn (3), both $I_{RA(off)}$ and $I_{RA(on)}$ should be pure Rayleigh-scattering signals; in other words, the contribution of stray light to the central-spectral-channel signal must be subtracted. It should be pointed out also that Eqns. (1) and (2) for the determination of T_e and n_e are valid only when the so-called scattering parameter α is much smaller than 1 [3].

39]. Otherwise a look-up table can be used to find the true T_e and n_e from the values of T_e and n_e calculated by using these two equations. For more detail about this data-treatment procedure, the reader is referred to a recent paper [40].

3. EXPERIMENTAL

The entire multichannel Thomson-scattering system constructed in our laboratory has been described previously [41]. In the present study, a commercial MAK torch with relatively low argon gas flow and RF input power was used. Two settings of ICP operating conditions used in the measurements are listed in Table 1. For these conditions, the tip of the "bullet" in the ICP is located at 2 mm ALC (0.75 kW) and 0 mm ALC (1.0 kW). In order to improve accuracy, the multichannel detector system was normalized by using a calibrated tungsten ribbon lamp, located exactly in place of the plasma. In earlier work [28,41], a light-emitting diode (LED) was mounted on the top of the focusing concave mirror inside the monochromator. Light emitted by the LED was used to illuminate directly the whole area of the fiber-optic array but without passing through any of the optical elements between the ICAP and the monochromator. In contrast, the light emitted by the tungsten ribbon lamp travels exactly the same path and illuminates the same portion of the fiber-optic array as does the scattered laser light. In addition, the illumination by the tungsten ribbon lamp also simulates a scattering signal well because it is pulsed by rotation of a mirror located in the light-collecting system. Of course the pulse length (about 25 μs) is much longer than that from the earlier LED (400 ns). During the experiment, the LED was still used to monitor the stability of each spectral channel. To compare the two approaches, the normalization factors for the first nine spectral

channels determined by the tungsten ribbon lamp and the LED, and their normalized ratios, are listed in Table 2.

Because the width and height of the monochromator entrance slit were set at 0.8 and 1.0 mm, respectively, and the optical collecting system has an image magnification of 1:1, the spatial resolution in our measurement was better than 1 mm^3. The temporal resolution is limited by the pulse length of the Q-switched ruby laser (~ 25 ns).

The stray-light contribution to the signal from the central spectral channel was determined by measuring the Rayleigh-scattering signals from argon and helium, respectively; both gases were at atmospheric pressure and at room temperature [35].

4. RESULTS

Radial profiles of T_e, n_e and T_g at five observation heights (5.0, 7.5, 10.0, 12.5 and 15.0 mm ALC) are shown in Figures 1-3 for 0.75 kW of RF input power. Similar profiles for 1.0 kW of RF input power are presented in Figures 4-6. In general, at each observation height, nine radial positions including the spatial point on the plasma axis were chosen with an increment between adjacent locations of 1.5 mm. Unfortunately, the electron number density drops rapidly with increasing observation height, particularly at larger radial distances from the plasma axis (see later discussion), resulting in very noisy Thomson scattering signals at the plasma edge. These noisy signals arise not only because the Thomson scattering signal is proportional to n_e, but also because stray light remains almost unchanged at the plasma edge, and the Rayleigh-scattering signal becomes even higher. This latter increase is due to the cooler gas temperature at the plasma boundary. As a result, at [illegible] data are shown in all Figs

[illegible] at 15.0 mm ALC, there are 5 data shown in Figures 4-6 (1.0 kW), but only 3 data in Figures 1-3 (0.75 kW), because the electron number density increases rapidly with RF input power (see later discussion).

It is appropriate to question whether the noisty Thomson signals at the plasma edge can be improved. The Thomson-scattering signals themselves are currently photon-noise limited. As a result, they can be improved only be acquiring larger numbers of photons. Importantly, this increase is not possible through use of a higher-power source laser, since a higher irradiance would perturb the plasma. Instead, it would be desirable to integrate a larger number of laser shots, possilby either by increasing the signal-integration interval or by using a laser with a higher pulse repetition rate. The latter strategy is, of course, the most attractive. The background noise at the plasma edge is greater than that in the plasma center, a fact which further degrades Thomson signals acquired there. Fortunately, the contribution of this noise to a multichannel Thomson spectrum arises as a shot-noise-limited background and, like the Thomson signal itself, can be improved by accumulating more laser shots.

From Figures 1 and 4, the radial distributions of T_e are fairly flat below 10 mm ALC for both RF input power settings, but become more bell-shaped at higher observation positions (cf. Figures 1 and 4). In contrast, T_g (Figures 3 and 6) decreases rapidly with increasing radial distance from the plasma axis even at low observation heights. Furthermore, T_g is usually about 1000 K to 2000 K lower than T_e at every plasma location. It is also apparent that the radial profiles of n_e are quite symmetric with respect to the plasma axis at almost all observation positions (cf. Figures 2 and 5). The value of n_e drops more rapidly with increasing radial distance from the plasma axis when the observation height becomes larger. None of the radial

distribution of T_e, n_e or T_g in Figures 1-6 shows a clear doughnut shape.

Generally, when the RF input power is raised from 0.75 to 1.0 kW, very little change in T_e is found at observation heights lower than 10 mm ALC. However, an apparent increase (about 500 K) in T_e occurs at higher observation positions. By comparison, the effect of RF input power on T_g can be clearly seen even at 5 mm and 7.5 mm ALC, particularly at the plasma edge. An obvious increase of n_e with RF input power can be seen at all spatial points, an effect which becomes even more significant higher in the plasma. A more detailed and quantitative discussion of these observations is given in the following section.

5. DISCUSSION AND CONCLUSIONS

Electron temperatures T_e as a function of observation height on the plasma axis are shown in Figure 7 for both settings of RF input power (open triangles: 0.75 kW, filled triangles: 1.0 kW). It can be seen that T_e does not change greatly with observation height from 7.5 mm to 15.0 mm ALC, and that increasing RF input power from 0.75 kW to 1.0 kW raises only slightly (less than 10%) the T_e value on the plasma axis.

Similar plots for gas temperatures T_g are shown in Figure 8 (filled triangles: 0.75 kW, open triangles: 1.0 kW). Compared to T_e, the T_g value on the plasma axis decreases more quickly with observation height for both settings of RF input power. Also, the increment in Tg when RF input power is raised from 0.75 kW to 1.0 kW is more (more than 20% at observation heights above 10 mm ALC) than that in T_e.

Figure 9 shows the variation in electron number density n_e on the plasma axis with observation height (filled circles: 0.75 kW, open circles: 1.0 kW). Clearly, n_e drops with observation height even more quickly than

does T_e (Figure 7) or T_g (Figure 8). (Note the logarithmic vertical axis on Figure 9). In addition, n_e is much more sensitive to the RF input power than either T_e or T_g, particularly in the upper observation regions. For example, at 1.0 kW the n_e value at 15 mm ALC is about twice that at 0.75 kW.

Vertical distributions of n_e at 3 mm off the plasma axis are plotted in Figure 10 for both settings of RF input power (filled circles: 0.75 kW, open circles: 1.0 kW). Obviously, all n_e values at 3 mm off the plasma axis are lower than their corresponding ones on the plasma axis (Figure 9). Furthermore, at 3 mm off the plasma axis, n_e declines with observation height more rapidly than occurs on the plasma axis (compare Figures 9 and 10), particularly at lower RF input power.

Now let us compare in more detail the electron temperatures and their corresponding gas temperatures, and see how different they are from each other. From Figures 7 and 8, the disparity between T_g and T_e exists at all observation heights, and is generally between 1000 K and 2000 K, as mentioned in section 4. Note also that a rise in RF input power reduces the deviation slightly.

A comparison of the vertical distribution of T_e and T_g at 1.0 kW of RF input power and at 3 mm off the plasma axis is shown in Figure 11. It is not surprising that the off-axis difference between T_g and T_e is greater than that on-axis (See Figures 7 and 8).

Another way to evaluate how far the plasma deviates from LTE is to compare the measured n_e with values calculated according to the Saha equation. Examples of such comparisons are given in Figures 12 and 13 for 0.75 kW and 1.0 kW of RF input power, respectively. In Figure 12, the filled circles are n_e data measured on the plasma axis directly by Thomson scattering, whereas the open circles are values calculated from the Saha

equation. The same is true in Figure 13 except that the data were measured at 3 mm off the plasma axis. From both figures, it can be seen that the apparent deviation of n_e from the LTE values (derived from T_e) exists at all observation heights. In general, this deviation ranges from a factor of 3 to one order of magnitude, depending on the spatial position and RF input power. Thus, electrons in the plasma are overpopulated compared to what T_e would predict, resulting in what can be viewed as a recombining plasma.

The values of T_e, n_e and T_g presented in Figures 1-6 are comparable to those reported previously by other authors [1,3-5,13-35]. Although the electron temperatures measured here are about 20% lower than those reported by Batal et al. [13,14], their observation location was lower (2 mm ALC) and their RF input power was higher (1.5 kW) than ours. Better agreement (within 10%) has been found between our T_e data and those recently reported by Davis and Du [16]. All these authors determined T_e by measuring the intensities of the argon emission line and the background at 430 nm. Lu et al.[17] more recently published T_e values measured by Langmuir probes in the ICP. Their results are found very close to ours with the same RF input power.

The electron number densities shown in Figures 2 and 5 range from 1 x 10^{14} to 7 x 10^{15} cm^{-3}, which are similar or comparable to those previously reported [5,13-27], except results from Langmuir-probe measurements, which seem somewhat too high [17]. In general, our n_e values are in better agreement with those derived from absolute continuum intensities [1,19], but somewhat higher than those measured by H_β line broadening at low observation positions [25,27]. The discrepancy might be due to the different torches and ICP operating conditions.

The gas temperatures cited in Figures 3 and 6 are in the range reported by other authors [1,18,29,31-34]. Interestingly, our data for T_g are in good agreement with those measured by Doppler broadening of emission lines [29,33,34], but are much higher than values derived from molecular rotational spectra [1,18,31,32]. This dissimilarity is not surprising, since our determination of T_g from Rayleigh scattering is based on the ideal gas law, which relates the gas pressure with the kinetic temperature and argon-atom number density in the plasma. Because the gas pressure (and therefore density) is produced by the translational moment of the plasma species, the T_g determined by Rayleigh scattering should be closer to the Doppler temperature than to the rotational temperature under non-LTE conditions. The lower rotational temperature suggests also that the transfer of particle kinetic energy to molecular rotational movement is a slower process in the ICP than is kinetic-energy transfer from electrons to argon atoms.

As mentioned above, the measured n_e is higher than the LTE value for n_e calculated from the measured T_e. Viewed differently, if one uses the measured n_e to determine T_e according to the Saha equation [42], the T_e would be overestimated. This fact can explain the recent findings of Blades et al. [42] about the deviations of the ICP from LTE, when they observed ion-atom emission-intensity ratios for Sr, Ca, Mg, Cd and Zn. They found that the experimental ratios $(I_i/I_a)_{exp}$ are several times lower than the LTE ratios $(I_i/I_a)_{LTE}$ at 1.0 kW of RF input power. The reason is that they used their measured n_e to determine T_e by assuming LTE conditions and then used those T_e and n_e values to calculate $(I_i/I_a)_{LTE}$. However, as verified here, the actual T_e is lower than the T_e value determined in their way, and the ionic levels are actually less populated. Therefore, the measured ion-atom

emission intensity ratios should be lower than the corresponding "LTE" values. The same reasoning leads to their conclusion that the experimental degree of ionization for the same elements is lower than that under "LTE" conditions. Clearly, both T_e and n_e should be measured independently but directly in order to better describe the excitation and ionization processes in the ICP.

The overpopulation of electrons in the analytical zone might be a significant non-LTE feature for analytes in the ICP, because it not only favors the excitation and ionization by direct electron impact and charge transfer, but also gives rise to overpopulated argon excited states and high-energy electrons through recombination and superelastic collision [43]. There are two possible reasons why electrons in the ICP are overpopulated. First, the ambipolar-diffusion process [44], which causes electron-ion pairs to migrate from the fireball to the cooler plasma regions, is faster than the thermal-conduction process that leads to the transfer of kinetic energy from the fireball to the cooler plasma regions. As a consequence, the analytical zone gains electrons faster than it is heated thermally, resulting in an electron number density that is higher than the LTE value. Secondly, when the plasma travels upward, the argon ion-electron recombination process is relatively slow [45], compared to the plasma cooling caused by energy loss through thermal conduction, convection and radiation. Thus, electrons remain overpopulated and the plasma remains in a recombining mode.

Finally, the fact that none of the radial profiles of T_e, n_e and T_g shown in Figures 1-6 are doughnut-shaped is probably due to the ICP operating conditions suggested by the manufacturer of the MAK torch (see Table 1). Because the central argon gas flow was only 0.5 l/min. and no aerosol was added, all the above-mentioned parameters would quickly peak on

the plasma axis. As a matter of fact, our observation region was in the normal analytical zone, whereas the initial radiation zone was found far lower in the plasma (no sample aerosol was used in this study).

We conclude that, under our experimental conditions, (1) T_g in the ICP is about 1000 to 2000 K lower than T_e, and n_e is overpopulated by a factor of 3^{-10} compared to the LTE value determined by T_e; (2) n_e is most sensitive of the three variables to RF input power and to spatial position; (3) fast ambipolar diffusion and slow argon ion-electron recombination probably lead to the overpopulation of electrons, resulting in a recombining plasma in the analytical zone; (4) the ambipolar-diffusion and thermal-conduction processes are fast enough to cause rapid plasma decay; (5) T_e, n_e and T_g are the most important parameters to describe the non-LTE features of the ICP, and all these parameters can be simultaneously determined by Thomson scattering and Rayleigh scattering on a spatially and temporally resolved basis.

ACKNOWLEDGMENT

Supported in part by the National Science Foundation through grant CHE 87-22639, by the Office of Naval Research, and by BP America.

REFERENCES

1. G.R. KORNBLUM and L. de GALAN, *Spectrochim. Acta* 32B, 71 (1977).
2. P.W.J.M. BOUMANS and F.J. DE BOER, *Spectrochim. Acta* 32B, 365 (1977).
3. D.J. KALNICKY, V.A. FASSEL and R.N. KNISELEY, *Appl. Spectrosc.* 31, 137 (1977).
4. J. JAROSZ, J.M. MERMET and P.J. ROBIN, *Spectrochim. Acta* 33B, 55 (1978).
5. J.F. ALDER, R.M. BOMBELKA and G.F. KIRKBRIGHT, *Spectrochim. Acta* 35B, 163 (1980).
6. M. MITCHNER and C.H. KRUGER, *Partially Ionized Gases*. Wiley, New York (1973).
7. H. YASUDA and T. SEKIGUCHI, *Jap. J. Appl. Phys.* 18, 2245 (1979).
8. R.J. LOVETT, *Spectrochim. Acta* 37B, 969 (1982).
9. T. HASEGAWA and H. HARAGUCHI, *Spectrochim. Acta* 40B, 1067 (1985).
10. M. HUANG and G. HIEFTJE, Paper # 721 at 39th Pittsburgh Conference, New Orleans, LA, February (1988).
11. A. GOLDWASSER and J.M. MERMET, *Spectrochim. Acta* 41B, 725 (1986).
12. J.A.M. van der MULLEN, I.J.M.M. RAAIJMAKERS, A.C.A.P. van LAMMEREN, D.C. SCHRAM, B. van der SIJDE and H.J.W. SCHENKELAARS, *Spectrochim. Acta* 42B, 1039 (1987).
13. A. BATAL, J.JAROSZ and J.M. MERMET, *Spectrochim. Acta* 36B, 983 (1981).
14. A. BATAL, J.JAROSZ and J.M. MERMET, *Spectrochim. Acta* 37B, 511 (1982).

15. M. HUANG, K.A. MARSHALL and G.M. HIEFTJE, *Anal. Chem.* 58, 207 (1986).

16. J. DAVIES and C.M. DU, *J. Anal. Atom. Spectrosc.* 3, 433 (1988).

17. P. LU, P. GONG, T. LIN and R.S. HOUK, *Spectrochim. Acta* 43B, 273 (1988).

18. G.R. KORNBLUM and L. de GALAN, *Spectrochim. Acta* 29B, 249 (1974).

19. J.M. MERMET, *Spectrochim. ACTA* 30B, 383 (1975).

20. A. MONTASER, V.A. FASSEL and G. LARSEN, *Appl. Spectrosc.* 35, 385 (1981).

21. H. UCHIDA, K. TANABE, Y. NOJIRI, H. HARAGUCHI and K. FUWA, *Spectrochim. Acta* 36B, 711 (1981).

22. A. MONTASER and V.A. FASSEL, *Appl. Spectrosc.* 36, 613 (1982).

23. W.H. GUNTER, K. VISSER and P.B. ZEEMAN, *Spectrochim. Acta* 38B, 949 (1983).

24. B.L. CAUGHLIN and M.W. BLADES, *Spectrochim. Acta* 39B, 1583 (1984).

25. B.L. CAUGHLIN and M.W. BLADES, *Spectrochim. Acta* 40B, 987 (1985).

26. N. FURUTA, Y. NOKIRI and K. FUWA, *Spectrochim. Acta* 40B, 423 (1985).

27. E.H. CHOOT and G. HORLICK, *Spectrochim. Acta* 41B, 935 (1986).

28. K.A. MARSHALL and G.M. HIEFTJE, *Spectrochim. Acta* 43B, 841 (1988).

29. H.G.C. HUMAN and R.H. SCOTT, *Spectrochim. Acta* 31B, 459 (1976).

30. G.R. KORNBLUM and L. de GALAN, *Spectrochim. Acta* 30B, 511 (1976).

31. H. KAWAGUCHI, T. ITO and A. MIZUIKE, *Spectrochim. Acta* 36B, 615

(1981).

32. M.H. ABDALLAH and J.M. MERMET, *Spectrochim. Acta* 37B, 391 (1982).

33. T. HASEGAWA and H. HARAGUCHI, *Spectrochim. Acta* 40B, 123 (1985).

34. L.M. FAIRES, B.A. PALMER and J.M. BRAULT, *Spectrochim. Acta* 40B, 135 (1985).

35. K.A. MARSHALL and G.M. HIEFTJE, *J. Anal. At. Spectrom.* 2, 567 (1987).

36. D.E. EVANS and J. KATZENSTEIN, *Rep. Prog. Phys.* 32, 207 (1967).

37. J. SCHEFFIELD, *Plasma Scattering of Electromagnetic Radiation.* Academic Press, New York (1975).

38. A. SCHEELINE and M.J. ZOELLNER, *Appl. Spectrosc.* 38, 245 (1984).

39. M. HUANG and G.M. HIEFTJE, *Spectrochim. Acta* 40B, 1387 (1985).

40. M. HUANG and G.M. HIEFTJE, *Spectrochim. Acta* (in press, 1988).

41. K.A. MARSHALL and G.M. HIEFTJE, *Spectrochim. Acta* 43B, 851 (1988).

42. M.W. BLADES, B.L. CAUGHLIN, Z.H. WALKER and L.L. BURTON, *Prog. Analyt. Spectrosc.* 10, 57 (1987).

43. M. HUANG and G.M. HIEFTJE, Paper # 575 at 14th Annual Meeting of The Federation of Analytical Chemistry and Spectroscopy Societies, Detroit, MI, October (1987).

44. F. AESCHBACH, *spectrochim. Acta* 37B, 987 (1982)

45. D.C. SCHRAM, I.J.M.M. RAAIJMAKERS, B. van der SIJDE, H.J.W. SCHENKELLAARS, and P.W.J.M. BOUMANS, *Spectrochim. Acta* 38B, 1545 (1983).

Table 1 - ICP operating conditions

Torch	Commercial MAK torch	
RF Frequency	27.12 MHz	
RF input power	0.75 kW	1.0 kW
Outer argon flow	10.0 l/min	11.0 l/min
Intermediate argon flow	0.5 l/min	0.5 l/min
Central argon flow	0.5 l/min	0.5 l/min
Sample flow rate	none	none

Table 2. Comparison of Multichannel Normalization Factors Determined by Tungsten Ribbon Lamp (W) and Light Emitting Diode (LED)

Spectral channel number	1	2	3	4	5	6	7	8	9
Normalization factor (W)	14.36	10.48	9.14	30.30	5.48	10.97	12.68	8.05	4.08
Normalization factor (LED)	8.65	6.34	5.04	16.02	3.95	6.96	7.87	4.84	3.98
Ratio normalized to Channel 1	1.0	0.996	1.092	1.139	0.836	0.949	0.971	1.002	0.618

Figure Captions

Figure 1. Radial distributions of electron temperatures measured by Thomson scattering at five observation heights above the load coil and at an RF input power of 0.75 kW.

Figure 2. Radial distributions of electron number densities measured by Thomson scattering at five observation heights above the load coil and at an RF input power of 0.75 kW.

Figure 3. Radial distributions of gas kinetic temperatures measured by Rayleigh scattering at five observation heights above the load coil and at an RF input power of 0.75 kW.

Figure 4. Radial distributions of electron temperatures measured by Thomson scattering at five observation heights above the load coil and at an RF input power of 1.0 kW.

Figure 5. Radial distributions of electron number densities measured by Thomson scattering at five observation heights above the load coil and at an RF input power of 1.0 kW.

Figure 6. Radial distributions of gas kinetic temperatures measured by Rayleigh scattering at five observation

heights above the load coil and at an RF input power of 1.0 kW.

Figure 7. Electron temperatures on the plasma axis at five observation heights above the load coil and at an RF input power of 0.75 kW (open triangles) and 1.0 kW (filled triangles).

Figure 8. Gas temperatures on the plasma axis at five observation heights above the load coil and at an RF input power of 0.75 kW (filled triangles) and 1.0 kW (open triangles).

Figure 9. Electron number densities on the plasma axis at five observation heights above the load coil and at an RF input power of 0.75 kW (filled circles) and 1.0 kW (open circles).

Figure 10. Electron number densities at 3 mm off the plasma axis, at five observation heights above the load coil and at an RF input power of 0.75 kW (filled circles) and 1.0 kW (open circles).

Figure 11. Electron temperatures (open triangles) and gas-kinetic temperatures (filled triangles) at 3 mm off the plasma axis at five observation heights above the load coil and at an RF input power of 1.0 kW.

Figure 12. Electron number densities measured directly by Thomson scattering (filled circles) on the plasma axis at five

observation heights above the load coil and at RF input power of 0.75 kW, and the calculated LTE electron number densities (open circles), obtained from the Saha equation using the corresponding measured electron temperatures shown in Figure 7.

Figure 13. Electron number densities measured directly by Thomson scattering (filled circles) at 3 mm off the plasma axis at five observation heights above the load coil and at an RF input power of 1.0 kW, and the calculated LTE electron number densities (open circles), obtained from the Saha equation using the corresponding measured electron temperatures shown in Figure 11.

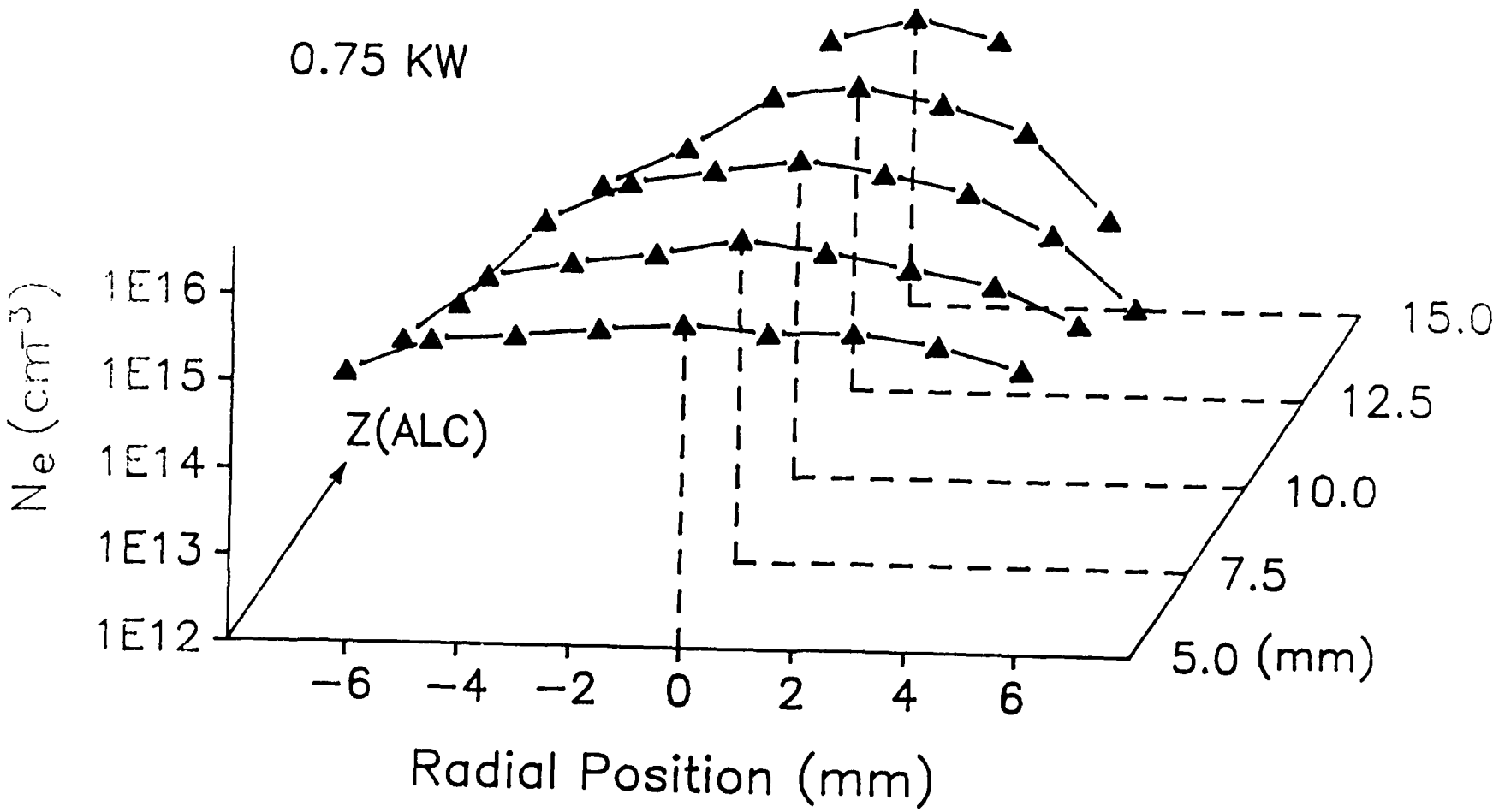
0.75 KW
Ne (cm⁻³)
1E16
1E15
1E14
1E13
1E12
Z(ALC)
15.0
12.5
10.0
7.5
5.0 (mm)
−6
−4
−2
0
2
4
6
Radial Position (mm)

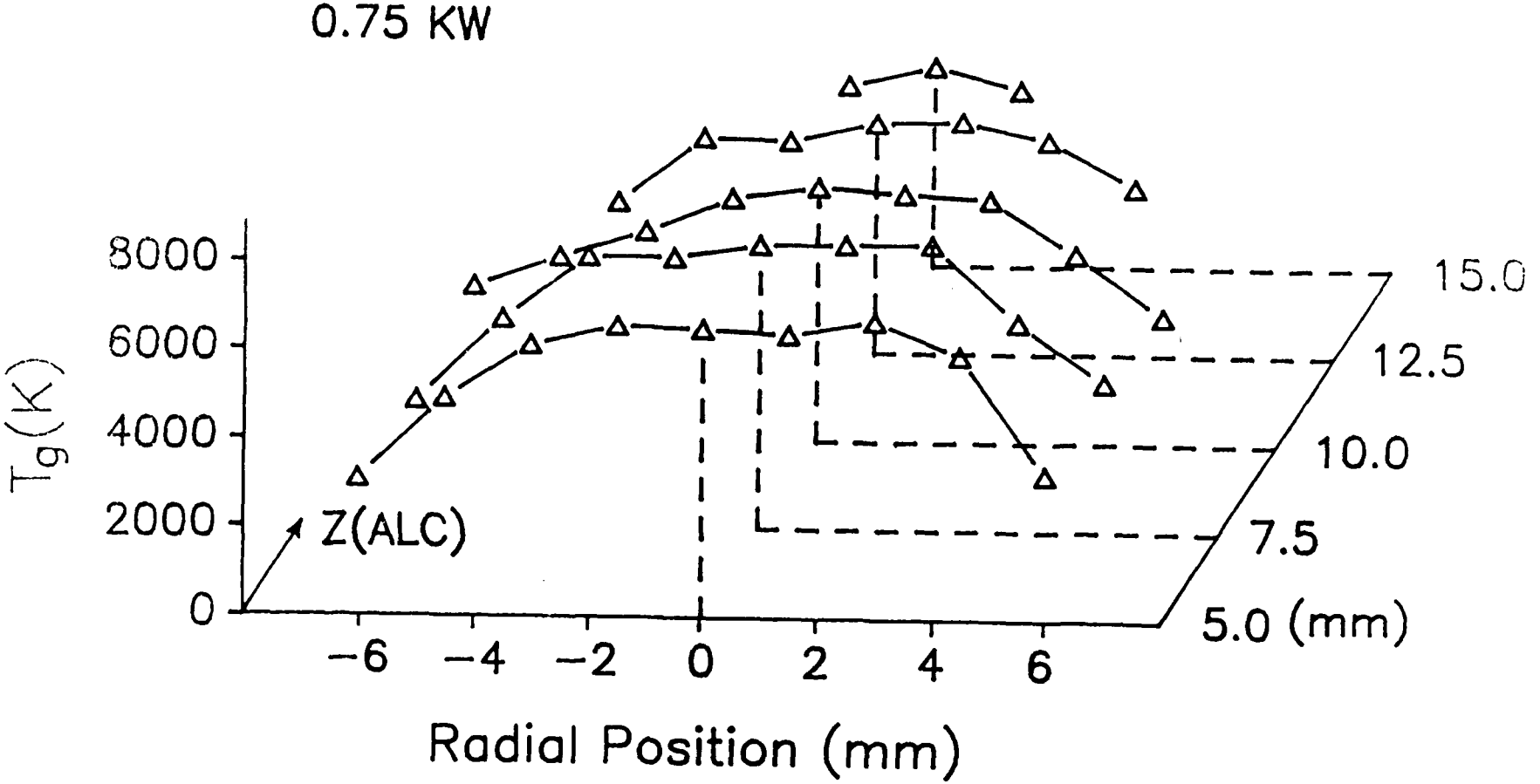
0.75 KW
8000
6000
4000
2000
0
T_g(K)
Z(ALC)
−6
−4
−2
0
2
4
6
Radial Position (mm)
15.0
12.5
10.0
7.5
5.0 (mm)

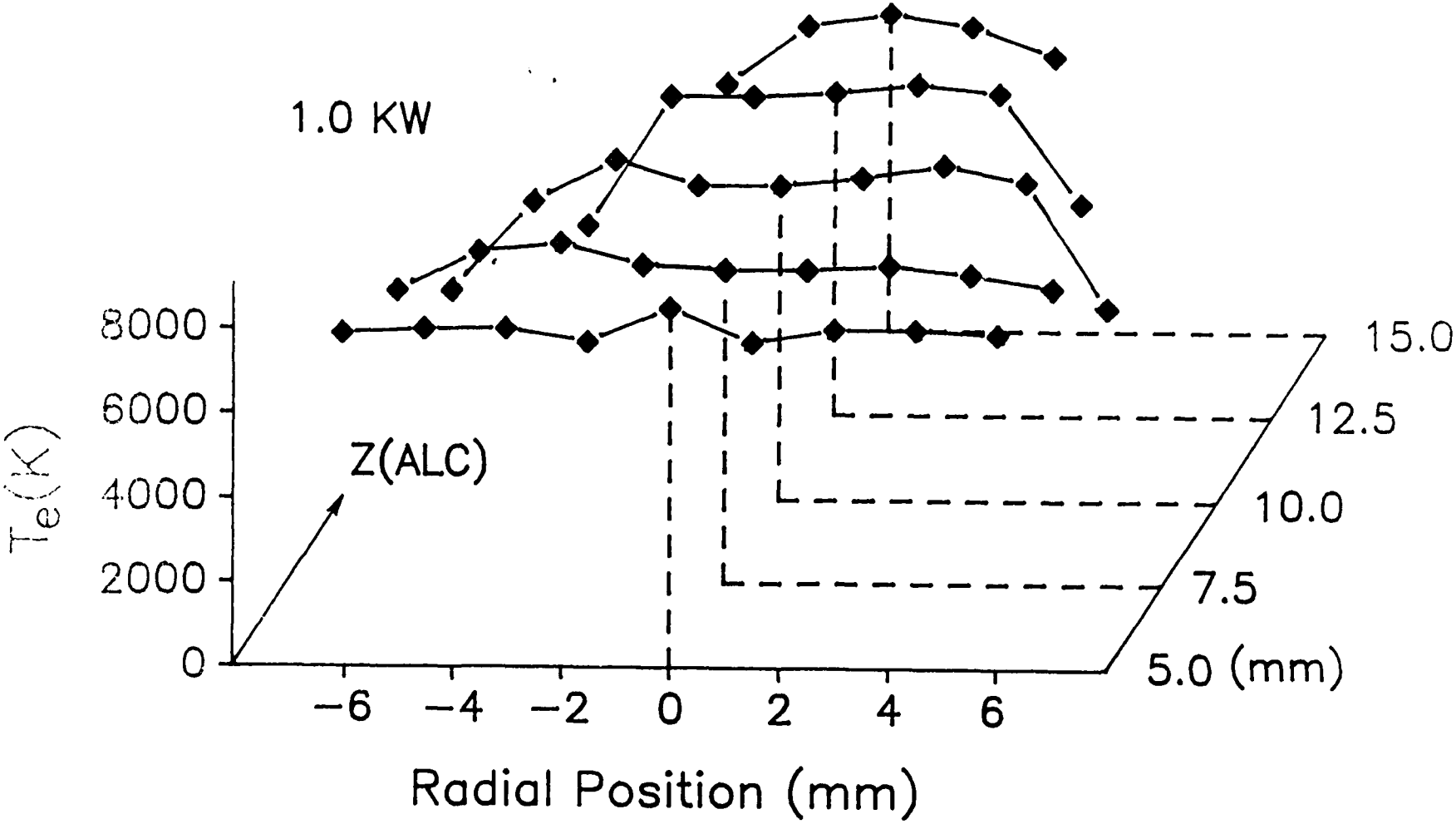
1.0 KW
8000
6000
4000
2000
0
T_e(K)
Z(ALC)
15.0
12.5
10.0
7.5
5.0 (mm)
−6
−4
−2
0
2
4
6
Radial Position (mm)

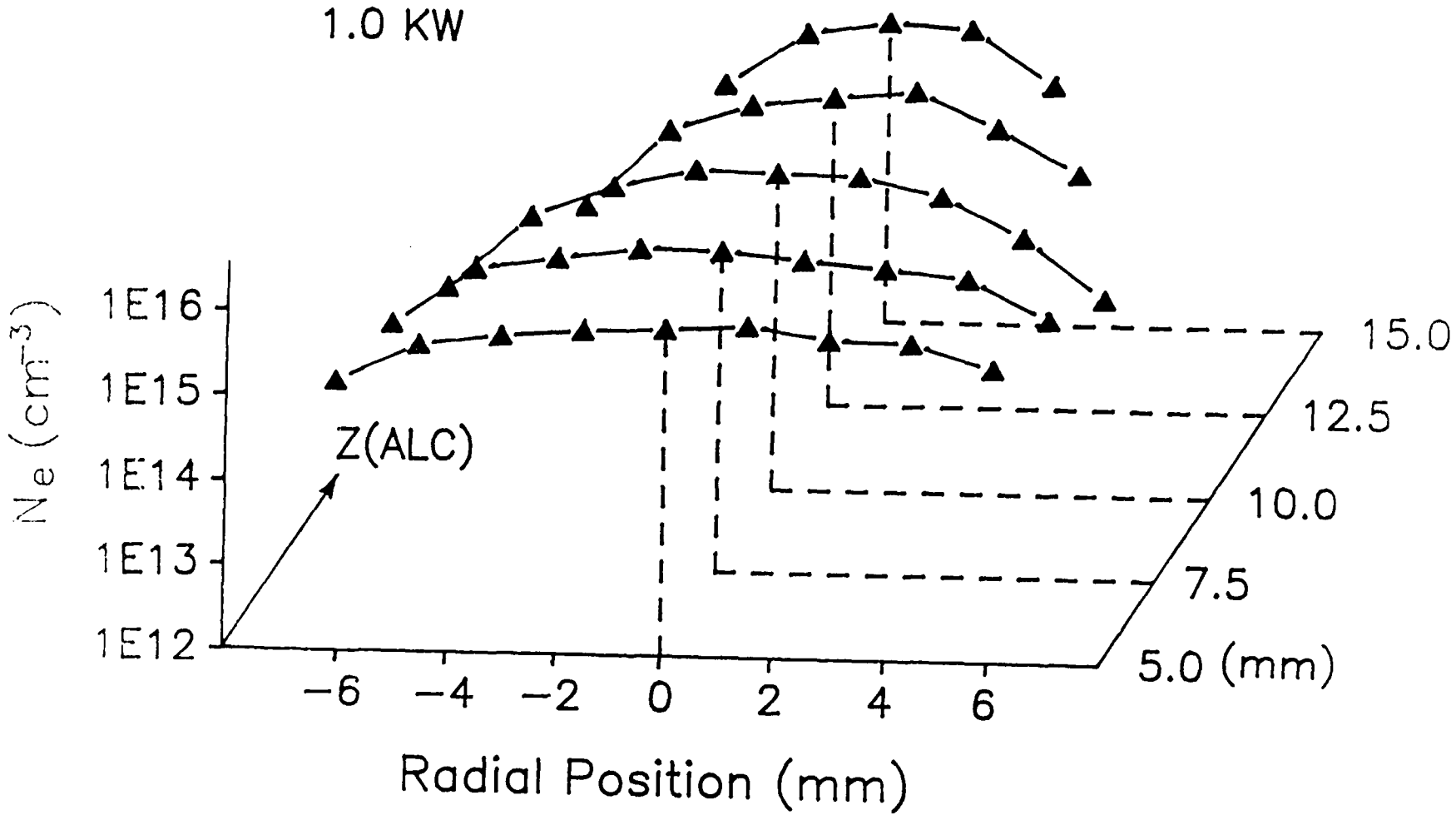
1.0 KW
N_e (cm^{-3})
1E16
1E15
1E14
1E13
1E12
Z(ALC)
15.0
12.5
10.0
7.5
5.0 (mm)
−6
−4
−2
0
2
4
6
Radial Position (mm)

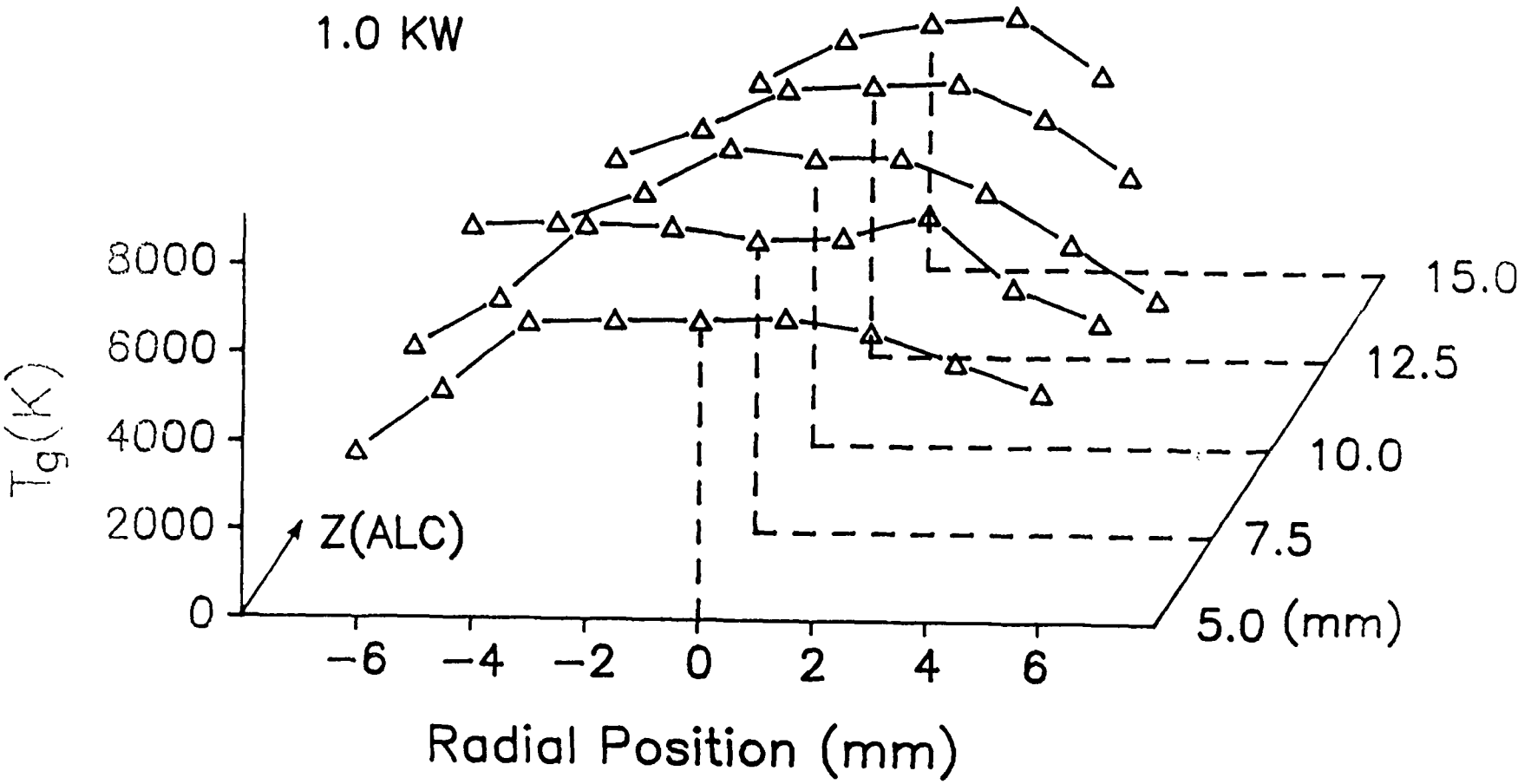
1.0 KW
8000
6000
4000
2000
0
T_g(K)
Z(ALC)
−6
−4
−2
0
2
4
6
Radial Position (mm)
15.0
12.5
10.0
7.5
5.0 (mm)

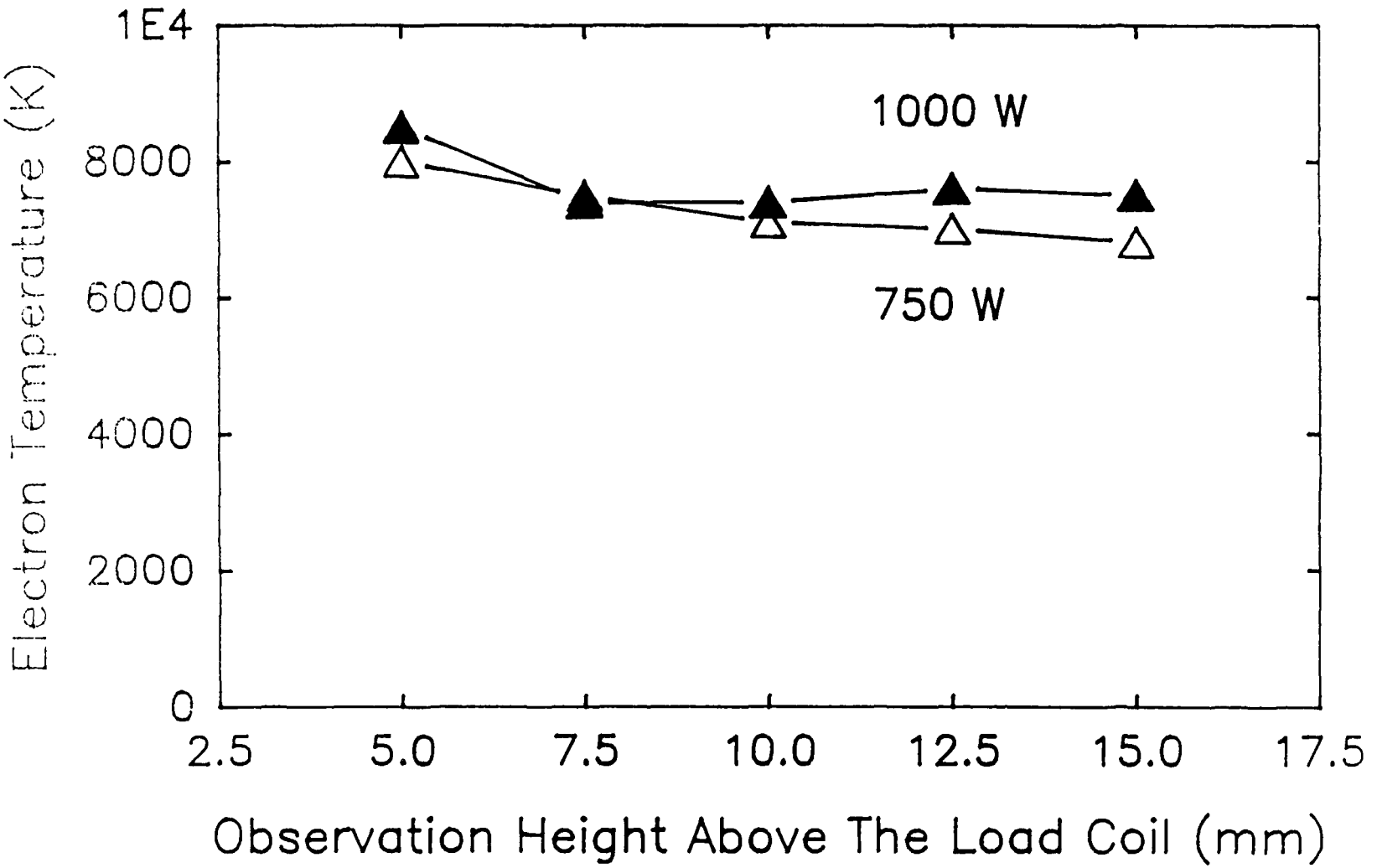
1E4
8000
6000
4000
2000
0
Electron Temperature (K)
1000 W
750 W
2.5
5.0
7.5
10.0
12.5
15.0
17.5
Observation Height Above The Load Coil (mm)

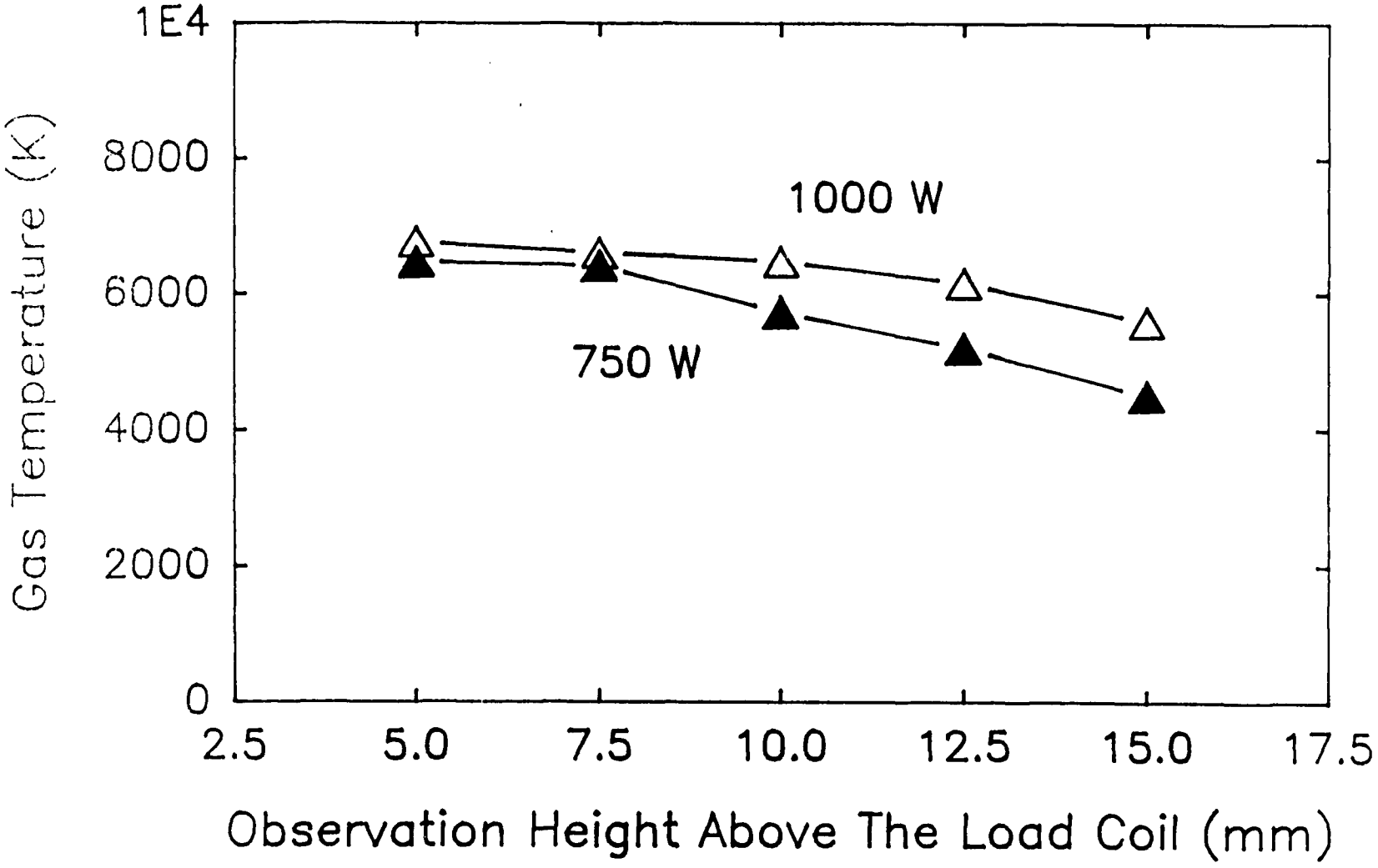
1E4
8000
6000
4000
2000
0
Gas Temperature (K)
1000 W
750 W
2.5
5.0
7.5
10.0
12.5
15.0
17.5
Observation Height Above The Load Coil (mm)

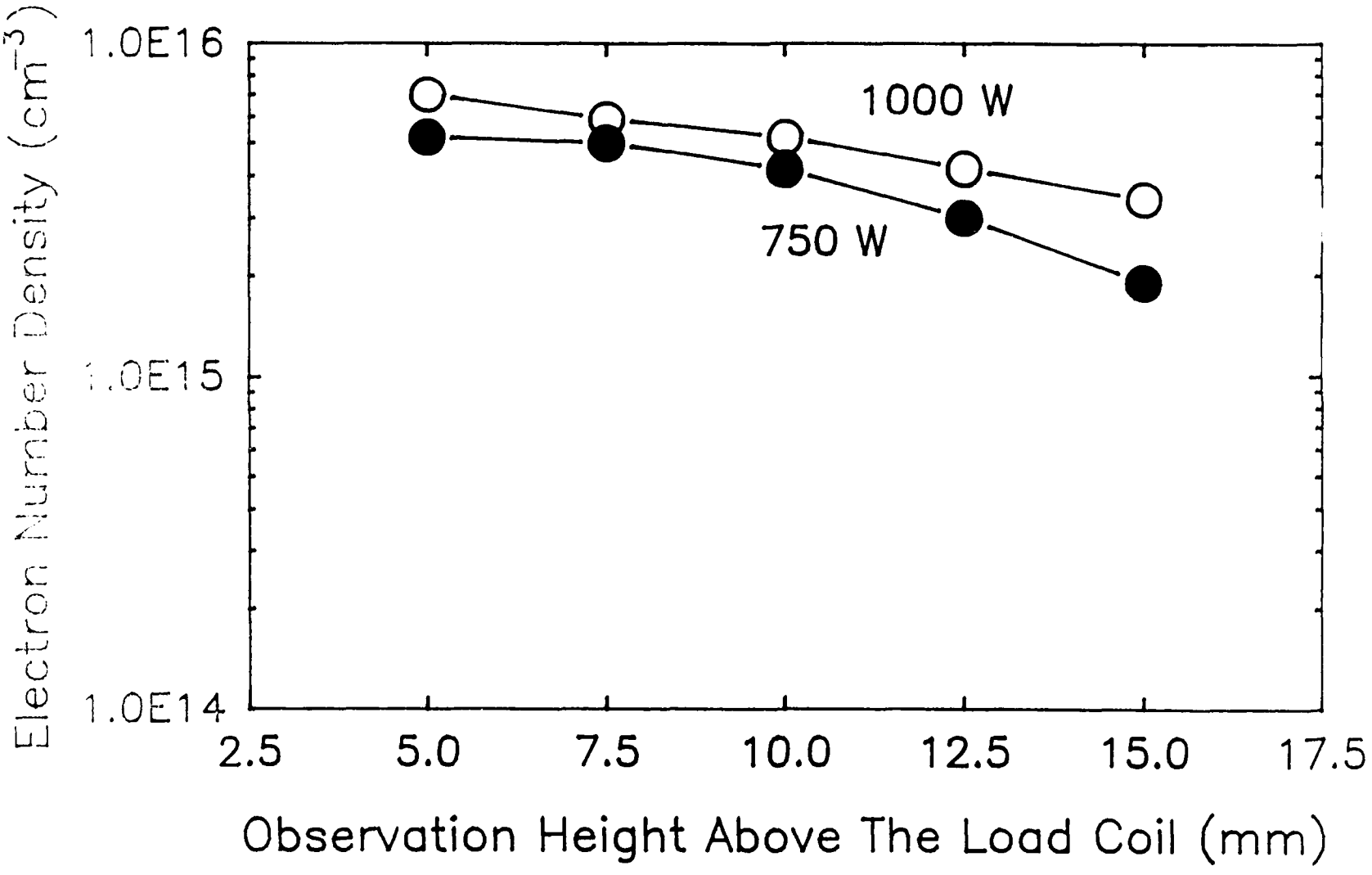
Electron Number Density (cm^{-3})
1.0E16
1.0E15
1.0E14
1000 W
750 W
2.5
5.0
7.5
10.0
12.5
15.0
17.5
Observation Height Above The Load Coil (mm)

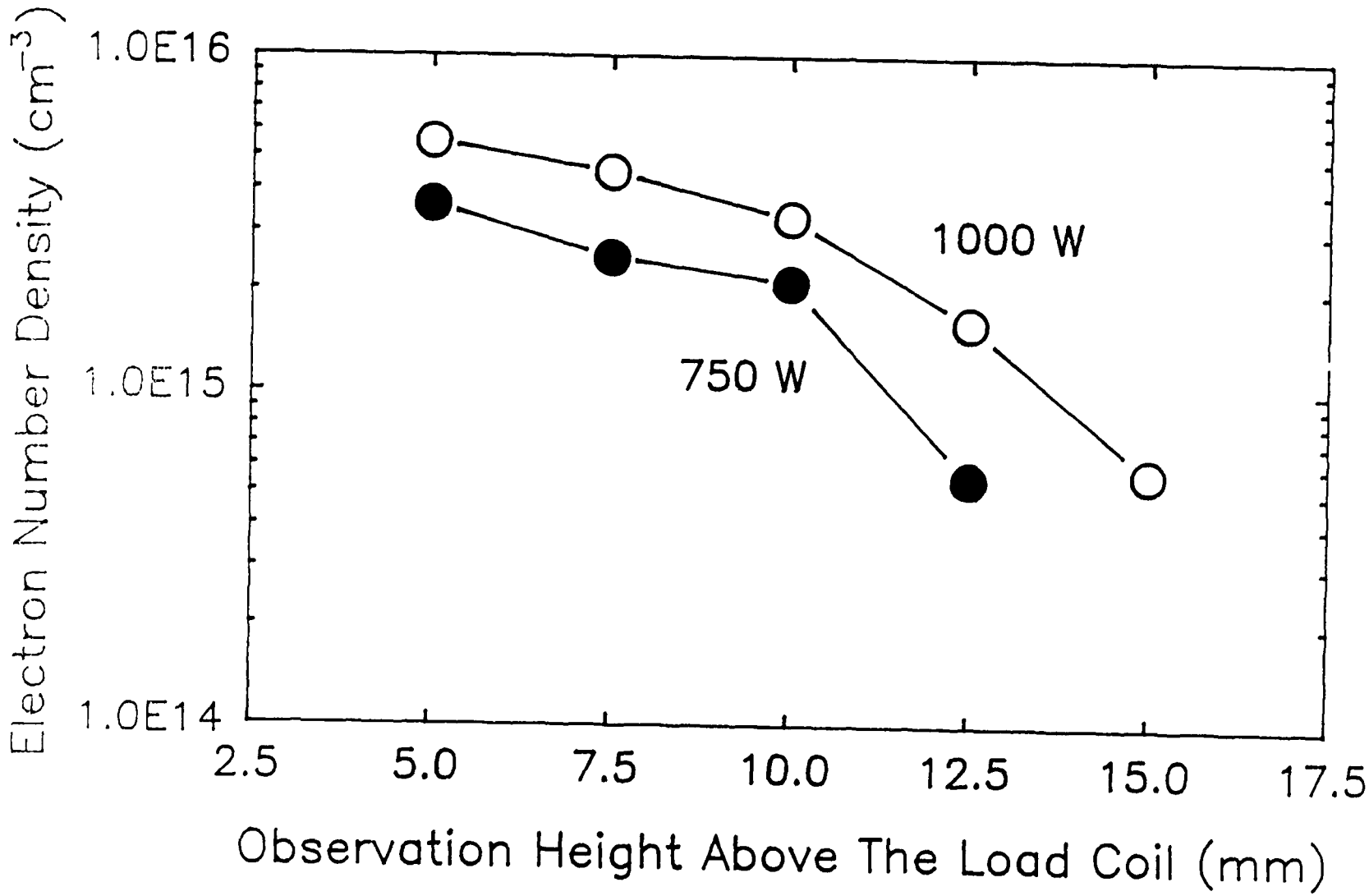
Electron Number Density (cm^{-3})
1.0E16
1.0E15
1.0E14
1000 W
750 W
2.5
5.0
7.5
10.0
12.5
15.0
17.5
Observation Height Above The Load Coil (mm)

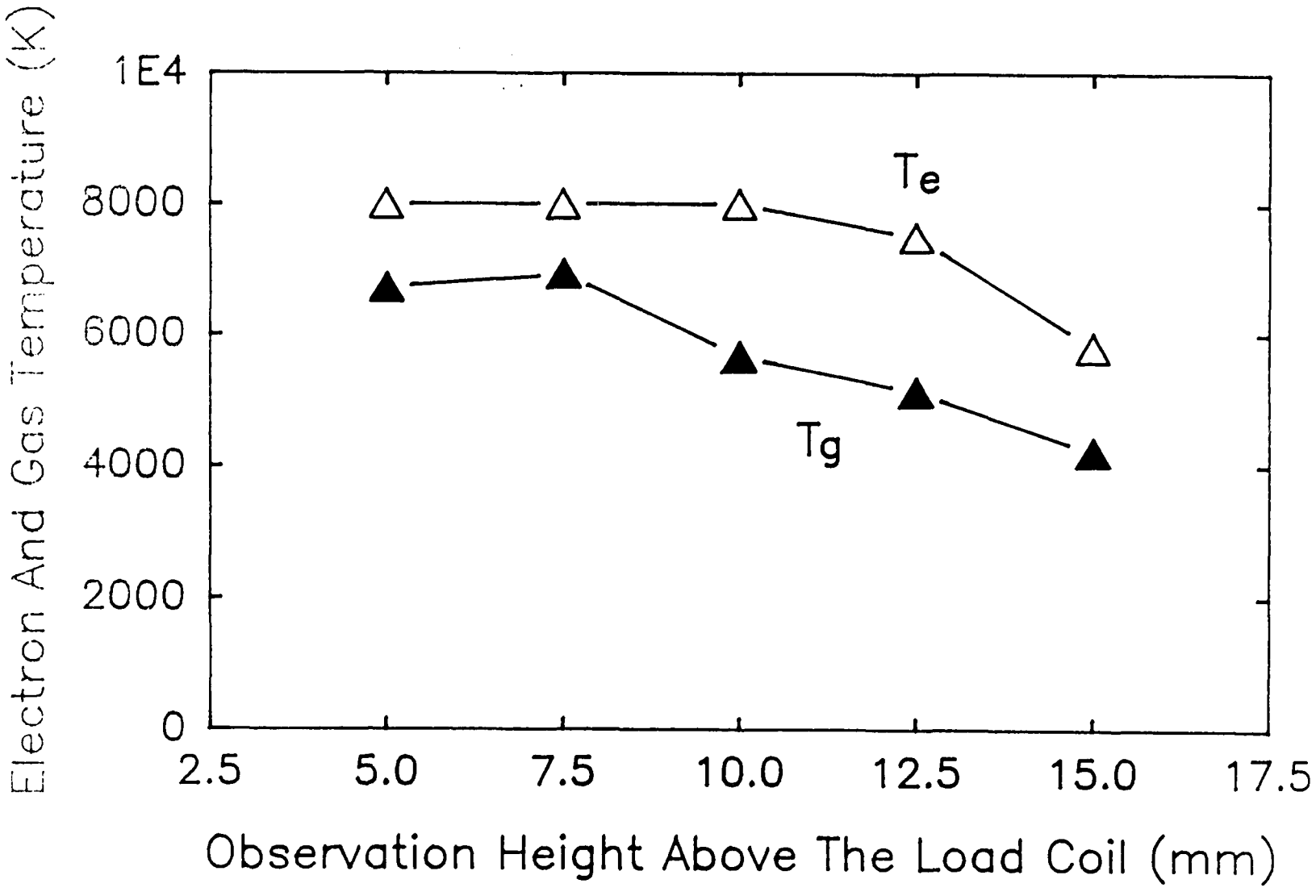
Electron And Gas Temperature (K)
1E4
8000
6000
4000
2000
0
Te
Tg
2.5
5.0
7.5
10.0
12.5
15.0
17.5
Observation Height Above The Load Coil (mm)

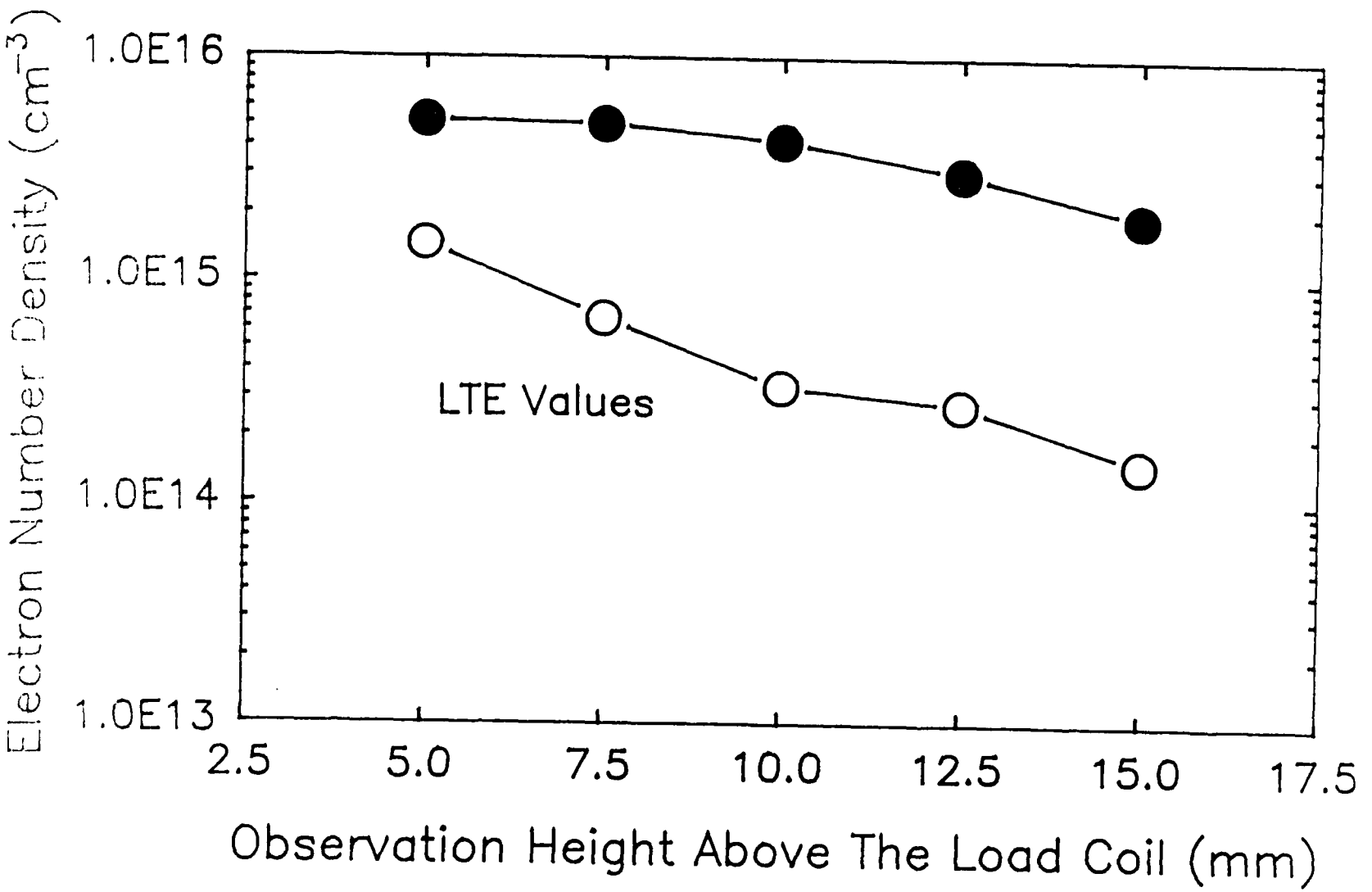
Electron Number Density (cm^{-3})
1.0E16
1.0E15
1.0E14
1.0E13
LTE Values
2.5
5.0
7.5
10.0
12.5
15.0
17.5
Observation Height Above The Load Coil (mm)

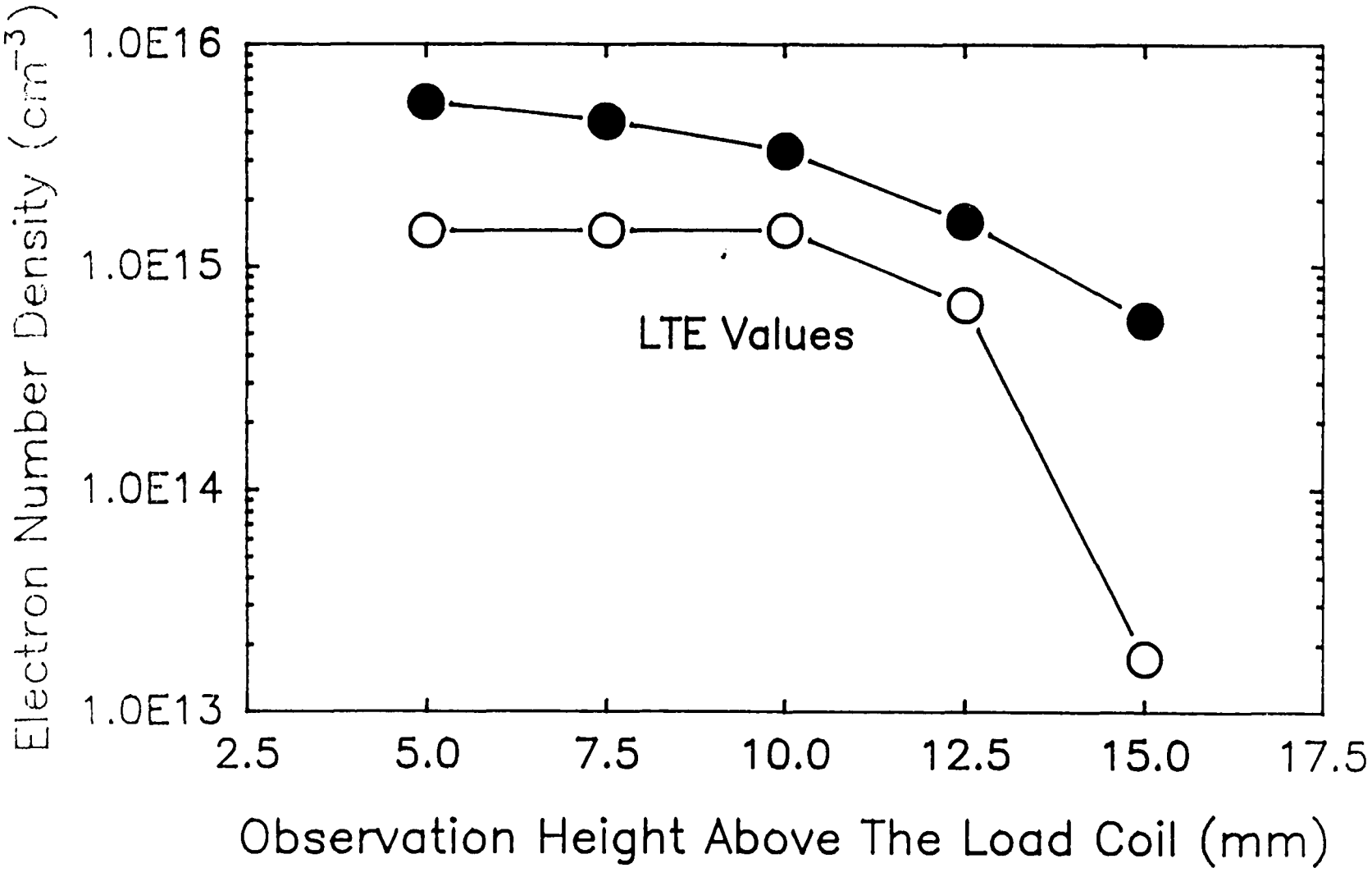
Electron Number Density (cm^{-3})
1.0E16
1.0E15
1.0E14
1.0E13
LTE Values
2.5
5.0
7.5
10.0
12.5
15.0
17.5
Observation Height Above The Load Coil (mm)